Supporting Information for

An intriguing window opened by a metallic two-dimensional Lindqvist-cobaltporphyrin organic framework as an electrochemical catalyst for the CO$_2$ reduction reaction

Cong Wang,[a] Chang-Yan Zhu,[a] Min Zhang,*[a] Yun Geng,[a] Yang-Guang Li[b] and Zhong-Min Su*[a,c]

[a.] Institute of Functional Material Chemistry, Faculty of Chemistry & National & Local United Engineering Laboratory for Power Battery, Northeast Normal University, 5268 Renmin Street, Changchun 130024, China.

[b.] Key Laboratory of Polyoxometalate Science of Ministry of Education, Faculty of Chemistry, Northeast Normal University, 5268 Renmin Street, Changchun 130024, China

[c.] School of Chemistry and Environmental Engineering, Changchun University of Science and Technology, 7989 Weixing Road, Changchun 130022, China.

*Emails: mzhang@nenu.edu.cn; zmsu@nenu.edu.cn

Table of contents

(Total Number of Pages: 25, Total Number of Figures: 17, Total Number of Tables: 4)

Model and Computational details

Model

A series of 2D TM-PMOF are constructed by linking reductive Lindqvist-type hexamolybdate ($[Mo_6]^{2e/2H}$) with 4-connected tetra-(4-aminophenyl) metalloporphyrin (TM-TAPP) building units through the Mo≡N triple bond (Fig. S1), where transition metals are common catalytic ones, including Fe, Co, Ni, Cu, Zn, Ru, Rh, Pd, Os, Ir, Pt. Typically, the interpenetrated topology might endow these structures with high chemical, thermal stability, and the direct connection of $[Mo_6]^{2e/2H}$ clusters with TM-TAPP ligands in a structure would presumably create an oriented electron transportation pathway under external driven voltage that might be beneficial for efficient charge transfer. A vacuum space of 30 Å in the z direction is adopted to avoid the interactions between the periodic layers.
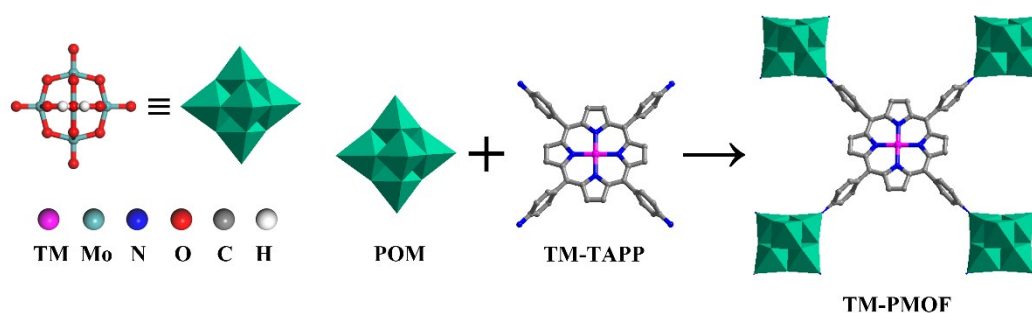
Fig. S1 Schematic illustration of the structure of 2D reductive TM-PMOF (TM = Fe, Co, Ni, Cu, Zn, Ru, Rh, Pd, Os, Ir, Pt).

Computational details

The spin-polarized density functional method within DMol³ code has been adopted for all calculations.[1,2] The Perdew-Burke-Ernzerhof (PBE) exchange-correlation functional of the generalized gradient approximation (GGA) was used for describing the electron interactions.[3] The DFT semi-core pseudopotential (DSPP) method was employed to consider the relativistic effects of transition metals, and the double numerical plus polarization (DNP) basis set was used for other elements.[4] The DFT-D2 method with the Grimme vdW correction was applied to describe the dispersion

interaction.[5] However, the calculations including Os, Ir, and Pt were performed without vdW corrections because of the lack of database. Self-consistent field (SCF) calculations were performed with a convergence criterion of 10^{-6} a.u. on the total energy and electronic computations. The conductor-like screening model (COSMO) was used to simulate a H_2O solvent environment throughout the whole process (dielectric constant: 78.54). The dipole correction was considered in all the calculations. The Brillouin zones were sampled with a $5 \times 5 \times 1$ k-point grid for geometry optimizations, whereas a $12 \times 12 \times 1$ grid was used for electronic structure computations. The Hirshfeld charge analysis was performed to study the charge transfer.[6] The thermodynamic stabilities of these TM-PMOFs were checked by performing *ab initio* molecular dynamics (AIMD) simulations at 300 K using the Nosé-Hoover heat bath scheme, in which the time step was set at 1.0 fs for a total period of 5 ps.

The adsorption energy (E_{ads}) for *CO intermediate on the 2D reductive TM-PMOF was defined as $E_{ads} = E_{TM-PMOF-CO} - E_{TM-PMOF} - E_{CO}$, where $E_{TM-PMOF-CO}$, $E_{TM-PMOF}$ and E_{CO} are the total energy for the total energy for the *CO adsorbed on the 2D reductive TM-PMOF, the pure 2D TM-PMOF, and the CO molecule, respectively. A negative value of the E_{ads} suggests favorable adsorption. The change in Gibbs free energy (ΔG) of every elemental step was acquired by applying the computational hydrogen electrode (CHE) model proposed by Nørskov et al.[7,8] In detail, the Gibbs free energy change is defined as $\Delta G = \Delta E + \Delta E_{ZPE} - T\Delta S + \Delta G_{pH} + \Delta G_U$, where ΔE is the electronic energy difference directly obtained by DFT calculations, ΔE_{ZPE} is the zero-point energy change, T is set at room temperature (298.15 K), and ΔS is the entropy change. The zero-point energies and entropies of adsorbed species were calculated from the vibrational frequencies, in which only the vibrational modes of adsorbate were calculated explicitly, while the catalyst substrate was fixed.[9-11] The entropies and vibrational frequencies of the free molecules were taken from the NIST database.[12] At the same time, the calculated energies, ZPE and TS of these free molecules are listed in Table S1. ΔG_{pH} is the free energy correction of pH, which can be calculated by $\Delta G_{pH} = 2.303k_BTpH$ (k_B is the Boltzmann constant, and the value of pH was set to zero for all

the calculations here). ΔG_U is the free energy contribution related to electrode potential (U), which can be determined as $\Delta G_U = - neU$, where n is the number of electrons transferred and U is the applied electrode potential.

Table S1. Energy data and correction of free molecules.

Free molecules	Energy (eV)	ZPE (eV)	TS (eV)	G (eV)
H_2 (g)	-31.82	0.26	0.40	-31.96
H_2O (l)	-2078.67	0.56	0.58	-2078.69
CO_2 (g)	-5128.84	0.31	0.66	-5129.19
CO (g)	-3180.25	0.13	0.61	-3180.73
HCHO (g)	-3113.74	0.70	0.68	-3113.72
CH_3OH (l)	-3146.80	1.35	0.74	-3146.19
CH_4 (g)	-1101.13	1.18	0.58	-1100.53
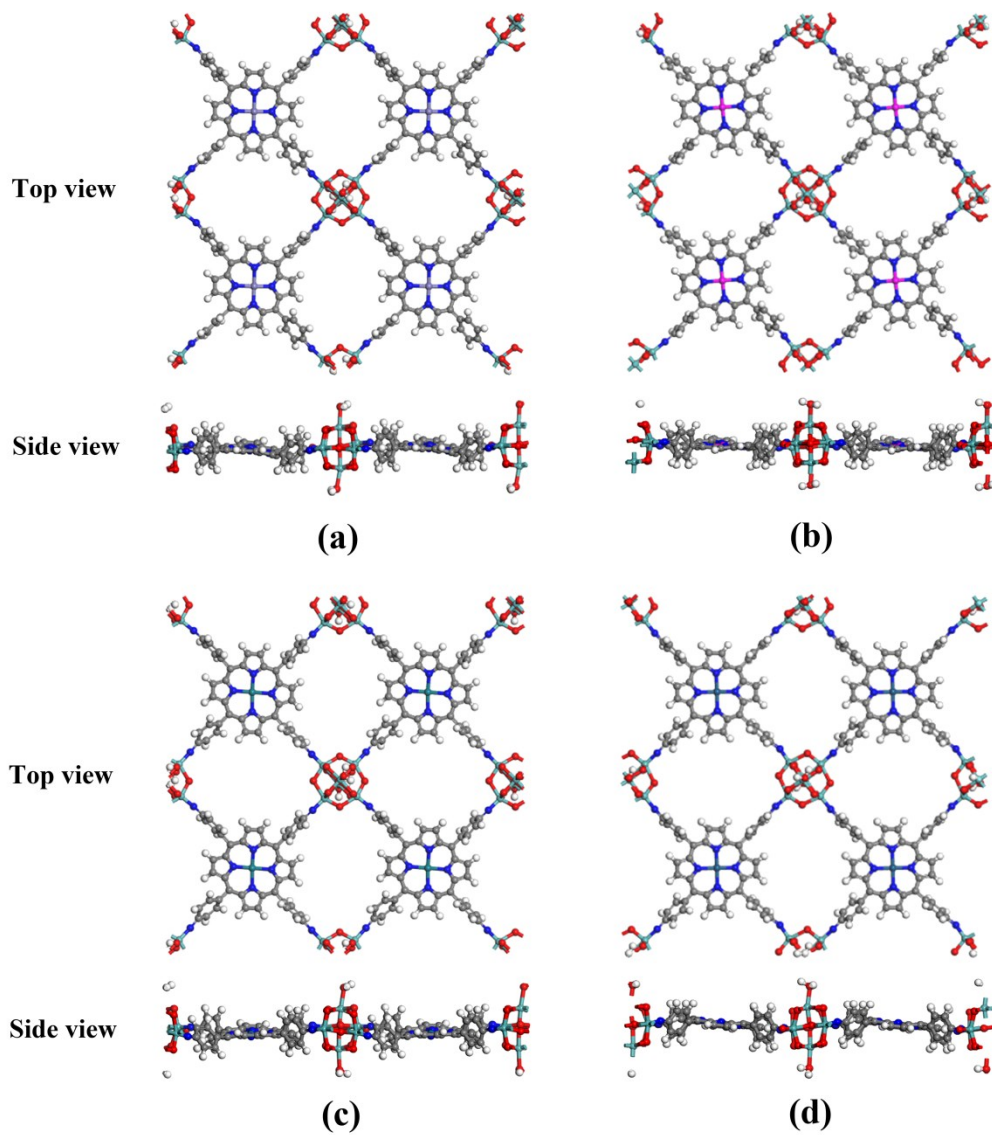
Fig. S2 The top and side views of the final structures of 2D reductive (a) Fe-PMOF, (b) Co-PMOF, (c) Rh-PMOF, and (d) Ir-PMOF at 300 K after 5000 steps of AIMD simulations.
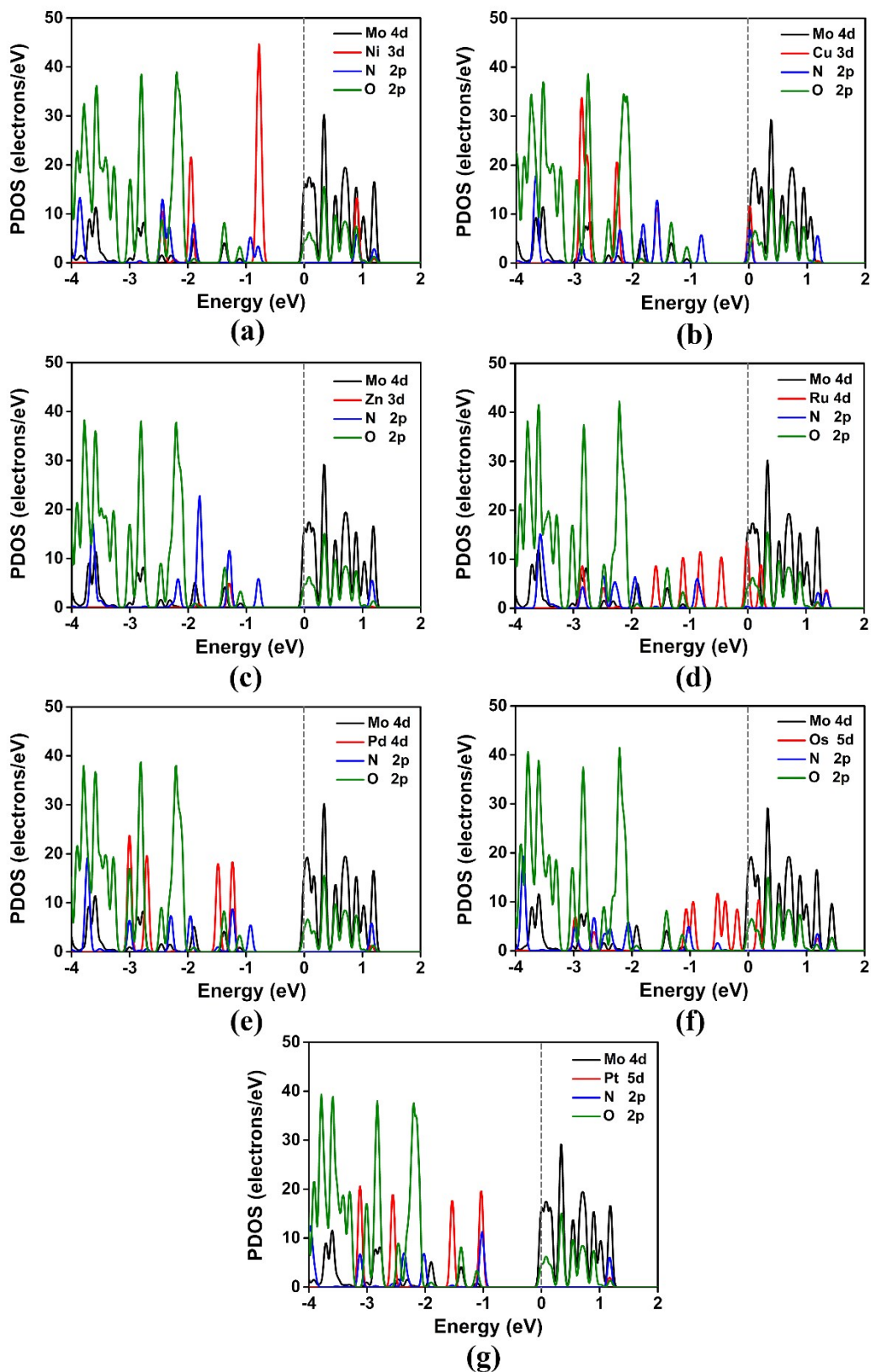
Fig. S3 The PDOS of 2D reductive (a) Ni-PMOF, (b) Cu-PMOF, (c) Zn-PMOF, (d) Ru-PMOF, (e) Pd-PMOF, (f) Os-PMOF and (g) Pt-PMOF.

To explore the best catalysts for CO_2 reduction, we analysed the PDOS of all reductive TM-PMOFs as shown in Fig. 4 and Fig. S3, separately. Firstly, according to the calculated PDOS results, we found that only the Fe-3d, Co-3d, Cu-3d, Ru-4d states originated from the central TM atoms in porphyrin rings cross the Fermi level, signifying that the 2D Fe-PMOF, Co-PMOF, Cu-PMOF, Ru-PMOF maybe possess high catalytic performance. Secondly, we know that if electron can be quickly transferred from the POM cluster to the central TM atom in porphyrin ring, the Mo-4d states originated from the $[Mo_6]^{2e/2H}$ clusters also needs to cross the Fermi level. Hence, the 2D Fe-PMOF does not have obvious advantages. Finally, we found that only the Mo-4d states originated from the $[Mo_6]^{2e/2H}$ clusters in 2D Co-PMOF within these TM-PMOFs cross the Fermi level and overlap with Co-3d states from cobaltporphyrin at the Fermi level to a higher density, which represents that the acquired electrons by the $[Mo_6]^{2e/2H}$ moiety can facilitate the transfer to the central Co atom in porphyrin rings due to their close energies and narrow distribution range. The feature ultimately benefits to a potentially high catalytic activity. Therefore, the Co-PMOF might be the best catalyst for CO_2 reduction based on the features of their PDOS.
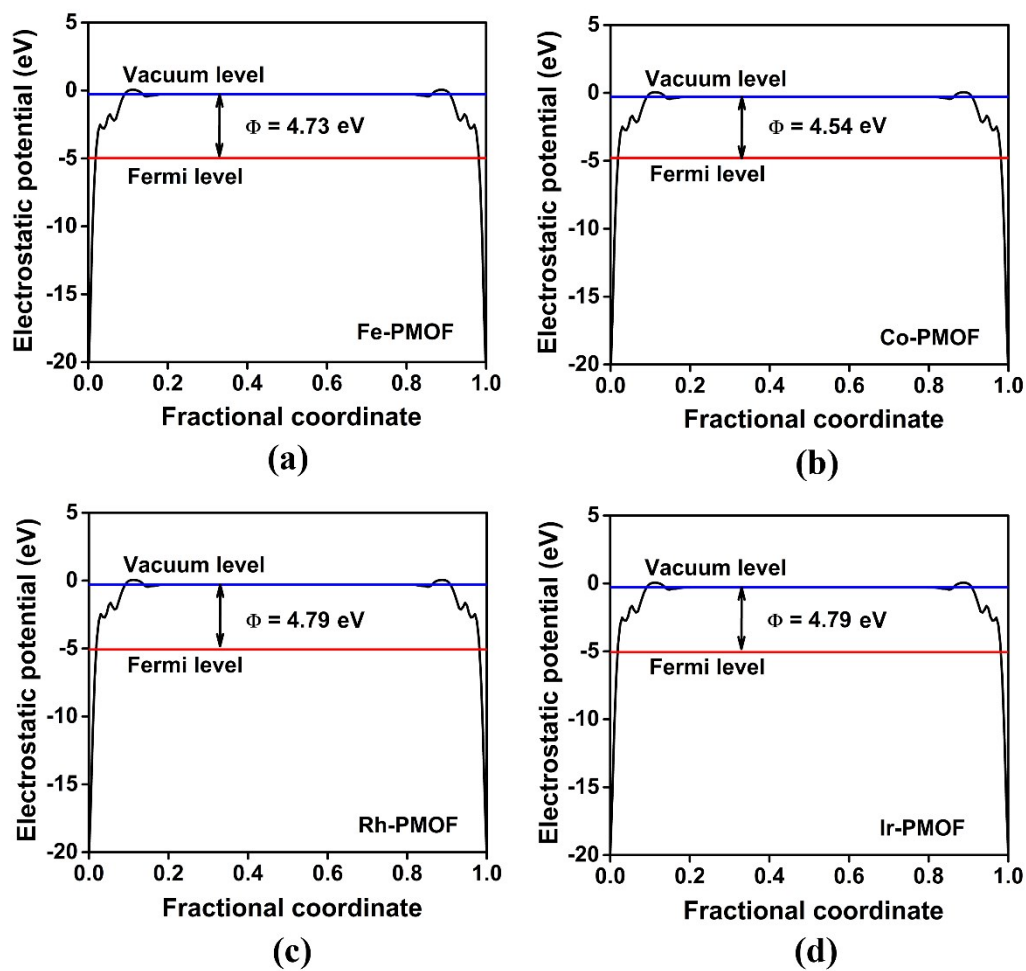
Fig. S4 The work functions of 2D reductive (a) Fe-PMOF, (b) Co-PMOF, (c) Rh-PMOF, and (d) Ir-PMOF.
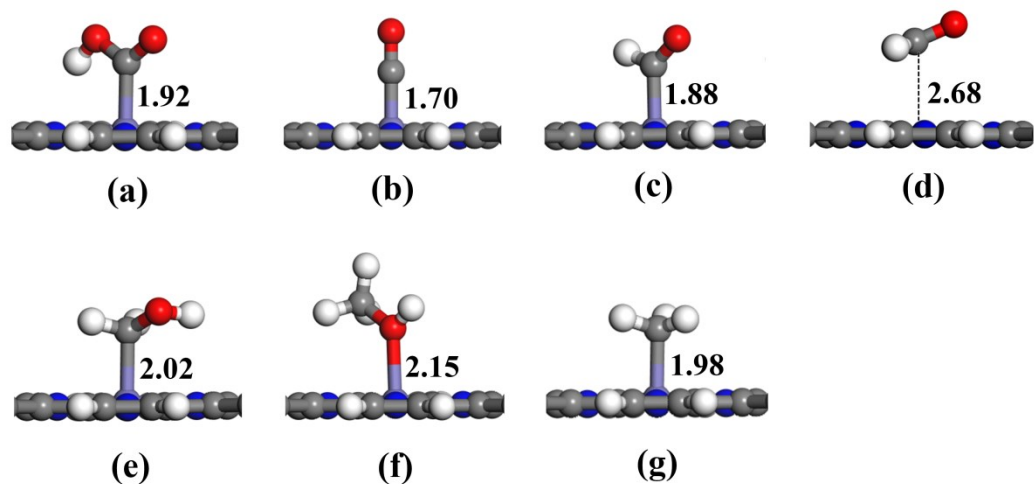
Fig. S5 The optimized structures of intermediates corresponding to the optimal hydrogenation path of the CO_2 on the 2D reductive Fe-PMOF: (a) *COOH, (b) *CO, (c) *CHO, (d) *CH_2O, (e) *CH_2OH, (f) *$OHCH_3$, (g) *CH_3. The bond length is labeled in Å.
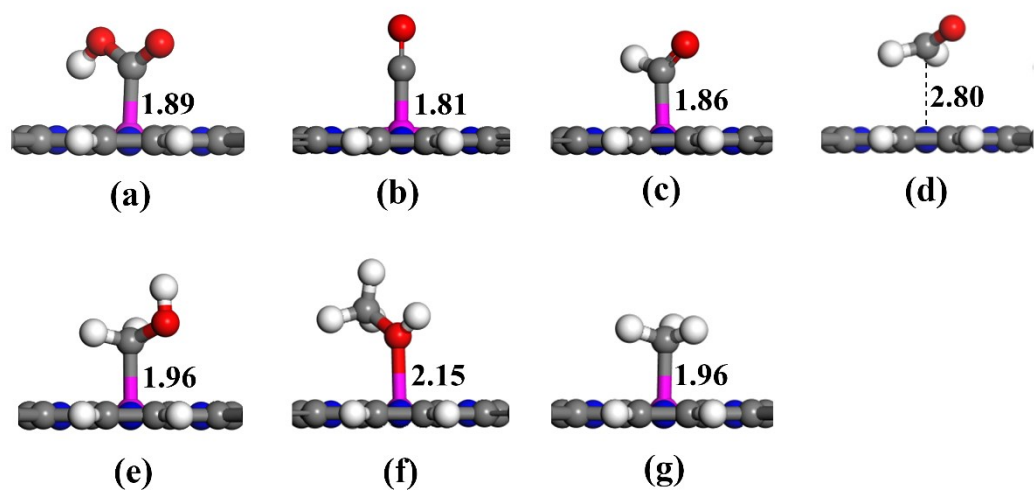
Fig. S6 The optimized structures of intermediates corresponding to the optimal hydrogenation path of the CO_2 on the 2D reductive Co-PMOF: (a) *COOH, (b) *CO, (c) *CHO, (d) *CH_2O, (e) *CH_2OH, (f) *$OHCH_3$, (g) *CH_3. The bond length is labeled in Å.
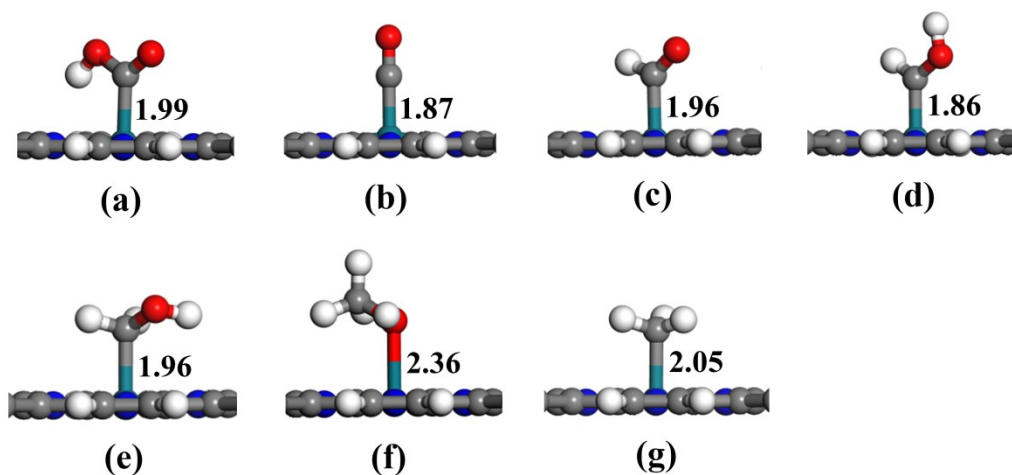
Fig. S7 The optimized structures of intermediates corresponding to the optimal hydrogenation path of the CO_2 on the 2D reductive Rh-PMOF: (a) *COOH, (b) *CO, (c) *CHO, (d) *CHOH, (e) *CH$_2$OH, (f) *OHCH$_3$, (g) *CH$_3$. The bond length is labeled in Å.

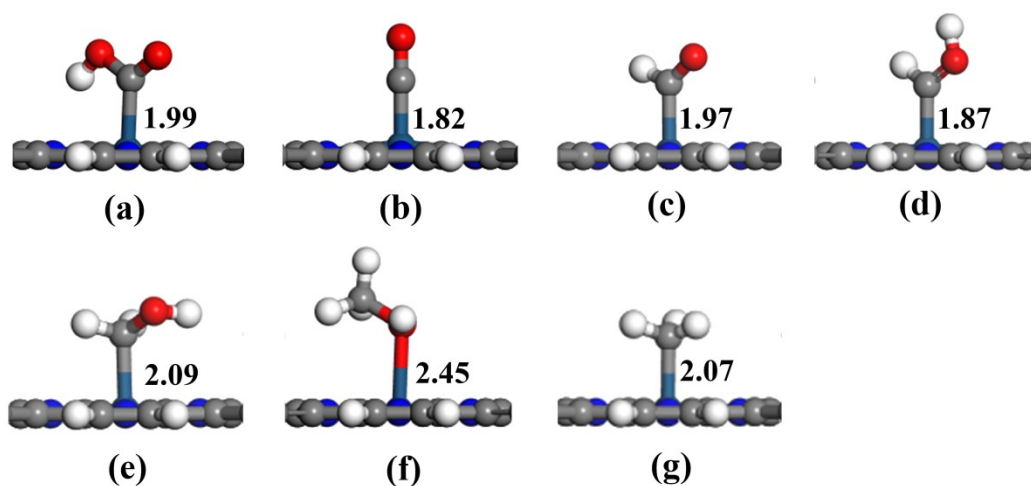**Fig. S8** The optimized structures of intermediates corresponding to the optimal hydrogenation path of the CO_2 on the 2D reductive Ir-PMOF: (a) *COOH, (b) *CO, (c) *CHO, (d) *CHOH, (e) *CH$_2$OH, (f) *OHCH$_3$, (g) *CH$_3$. The bond length is labeled in Å.

**The feasibility of the reduction to $[Mo_6]^{2e/2H}$ from $[Mo_6]$ in 2D Co-PMOF**

Considering the successful experimental synthesis of three-dimensional (3D) reductive polyoxometalate-metalloporphyrin organic frameworks constructed by reductive Zn-ε-Keggin clusters and metalloporphyrin linkers,[13,14] as well as the extensive application of highly active, reductive polyoxometalates in the field of electrocatalysis,[15,16] it is convinced that our proposed 2D reductive Co-PMOF structure is experimentally feasible and can be used as CO_2 reduction catalyst with excellent performance.. Here, to verify the feasibility of the reduction to $[Mo_6]^{2e/2H}$ from $[Mo_6]$ in 2D Co-PMOF, we calculate that the $[Mo_6]^{2e/2H}$ units inside are easily reduced from the $[Mo_6]$ with a low energy demand (0.08 eV), indicating that this reduction process is easy to occur.

Moreover, by analyzing the partial density of states (PDOS) diagrams of unreduced and reduced Co-PMOF (Fig. S10), we found that unreduced Co-PMOF is a narrow band gap semiconductor, and the reduced Co-PMOF has superior conductivity and potential electrocatalytic performance.

$+ H^+ + e^-$

(a)   (b)
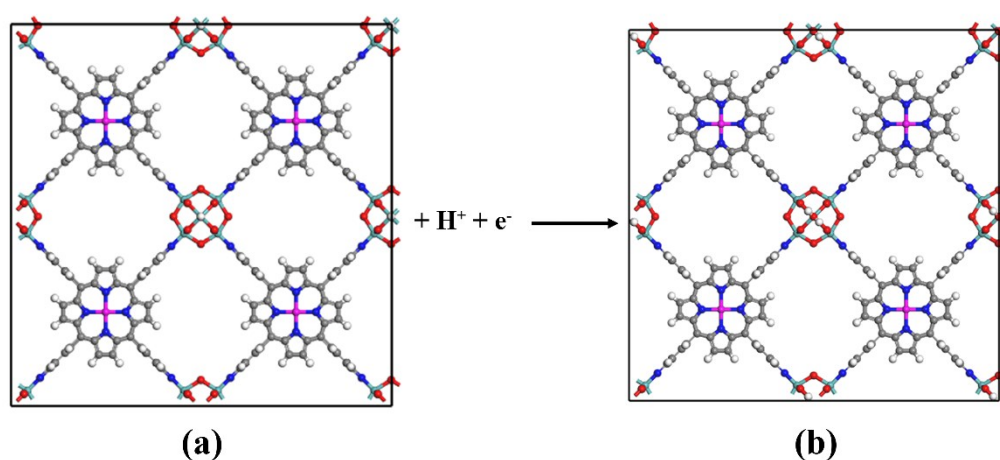
Fig. S9 Schematic diagrams of the reduction reaction of $[Mo_6]$ clusters in 2D Co-PMOF. $[Mo_6]$ experiences a two-electron/proton-coupled reduction to form $[Mo_6]^{2e/2H}$. The (a) and (b) denote the unreduced Co-PMOF and reduced Co-PMOF, respectively.
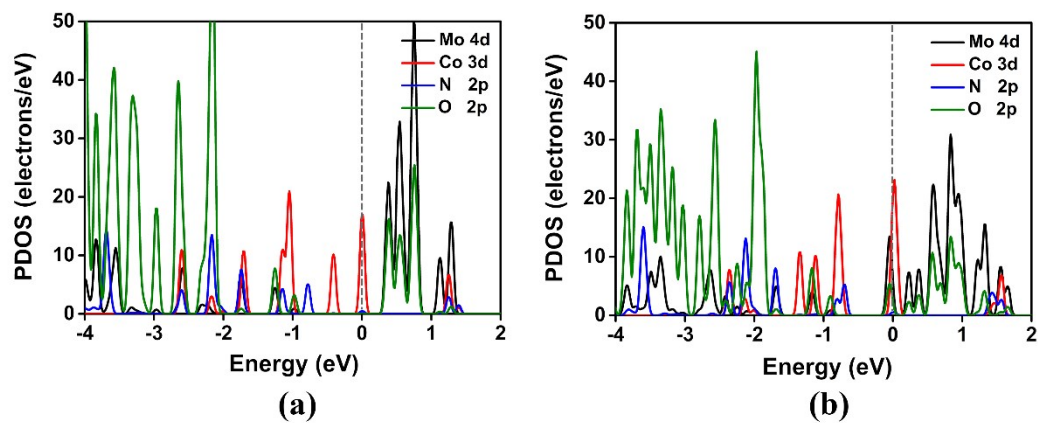
Fig. S10 The PDOS of (a) unreduced Co-PMOF and (b) reduced Co-PMOF.
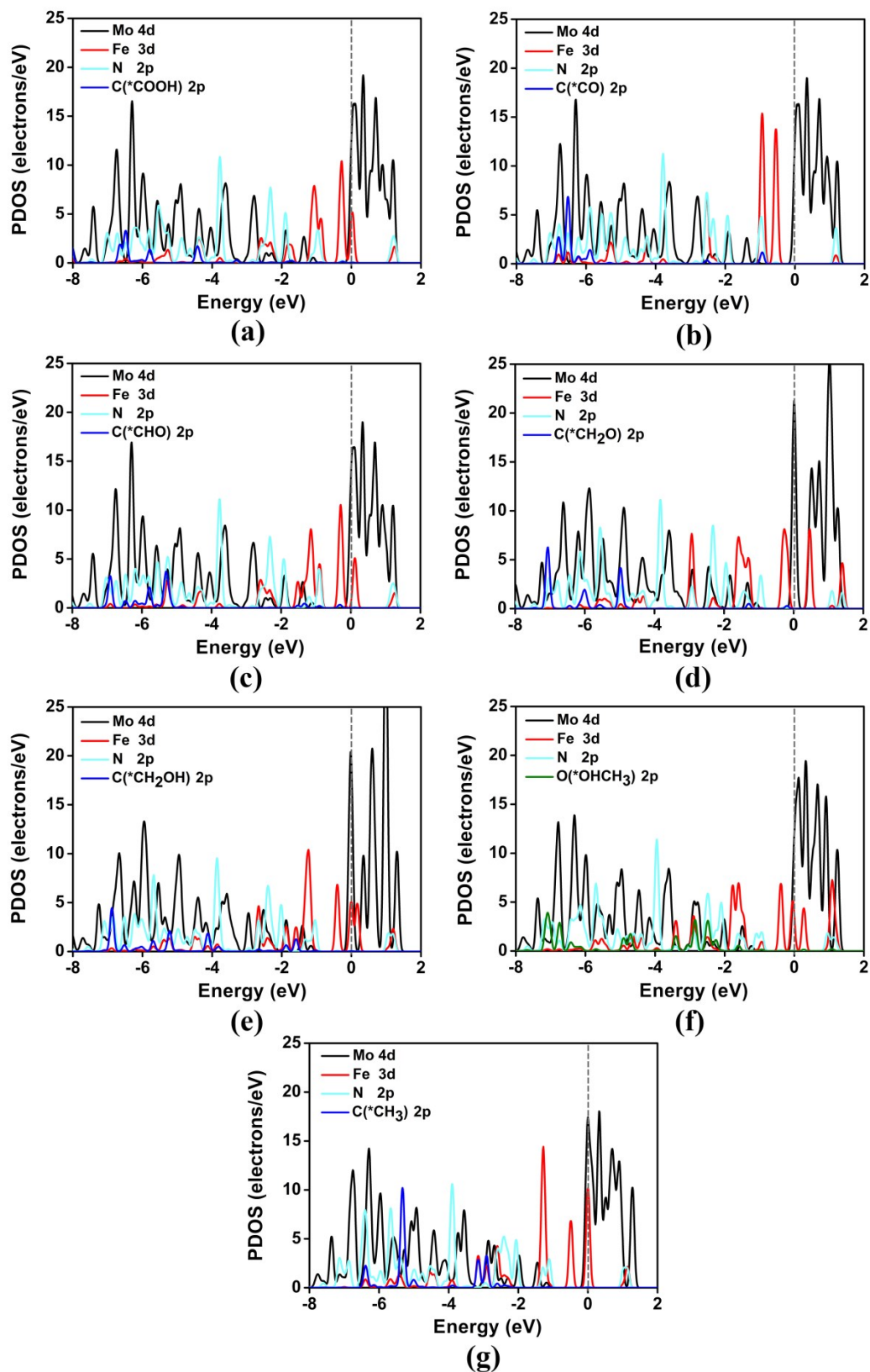
Fig. S11 The PDOS of 2D reductive Fe-PMOF adsorbing the intermediates of each step along the optimal reaction pathway: (a) *COOH, (b) *CO, (c) *CHO, (d) *CH$_2$O, (e) *CH$_2$OH, (f) *OHCH$_3$, (g) *CH$_3$.
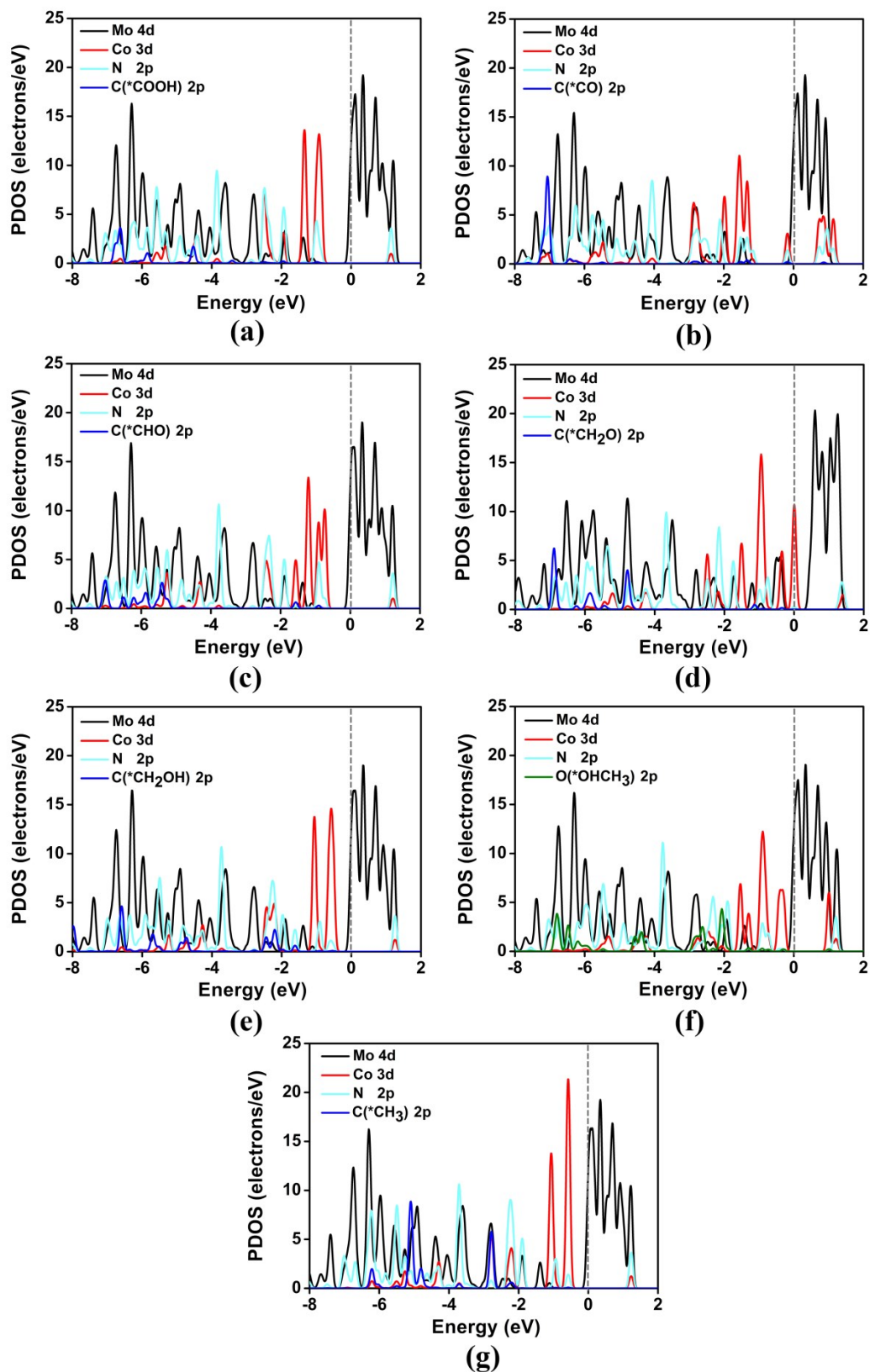
Fig. S12 The PDOS of 2D reductive Co-PMOF adsorbing the intermediates of each step along the optimal reaction pathway: (a) *COOH, (b) *CO, (c) *CHO, (d) *CH$_2$O, (e) *CH$_2$OH, (f) *OHCH$_3$, (g) *CH$_3$.
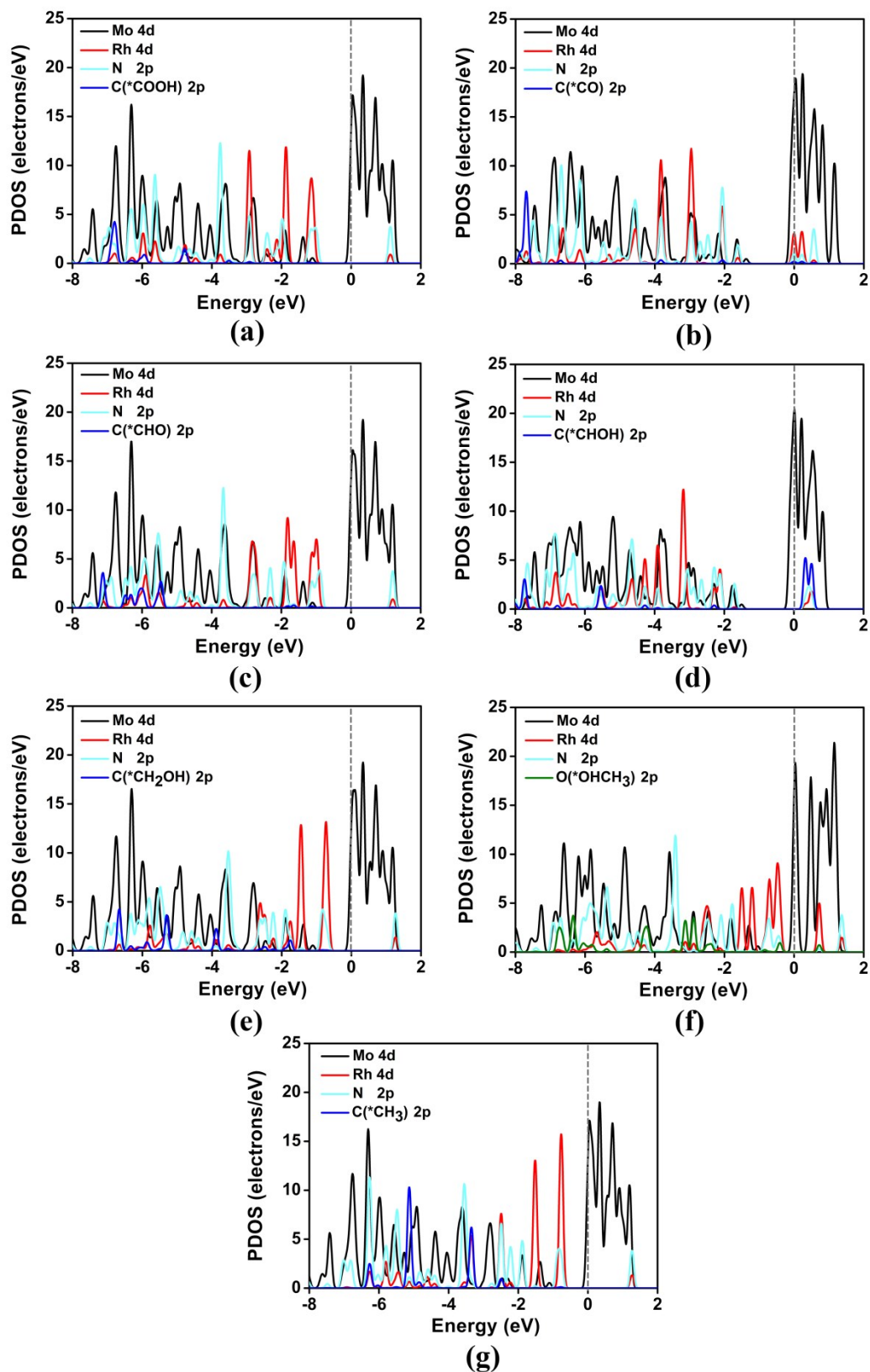
Fig. S13 The PDOS of 2D reductive Rh-PMOF adsorbing the intermediates of each step along the optimal reaction pathway: (a) *COOH, (b) *CO, (c) *CHO, (d) *CHOH, (e) *CH₂OH, (f) *OHCH₃, (g) *CH₃.
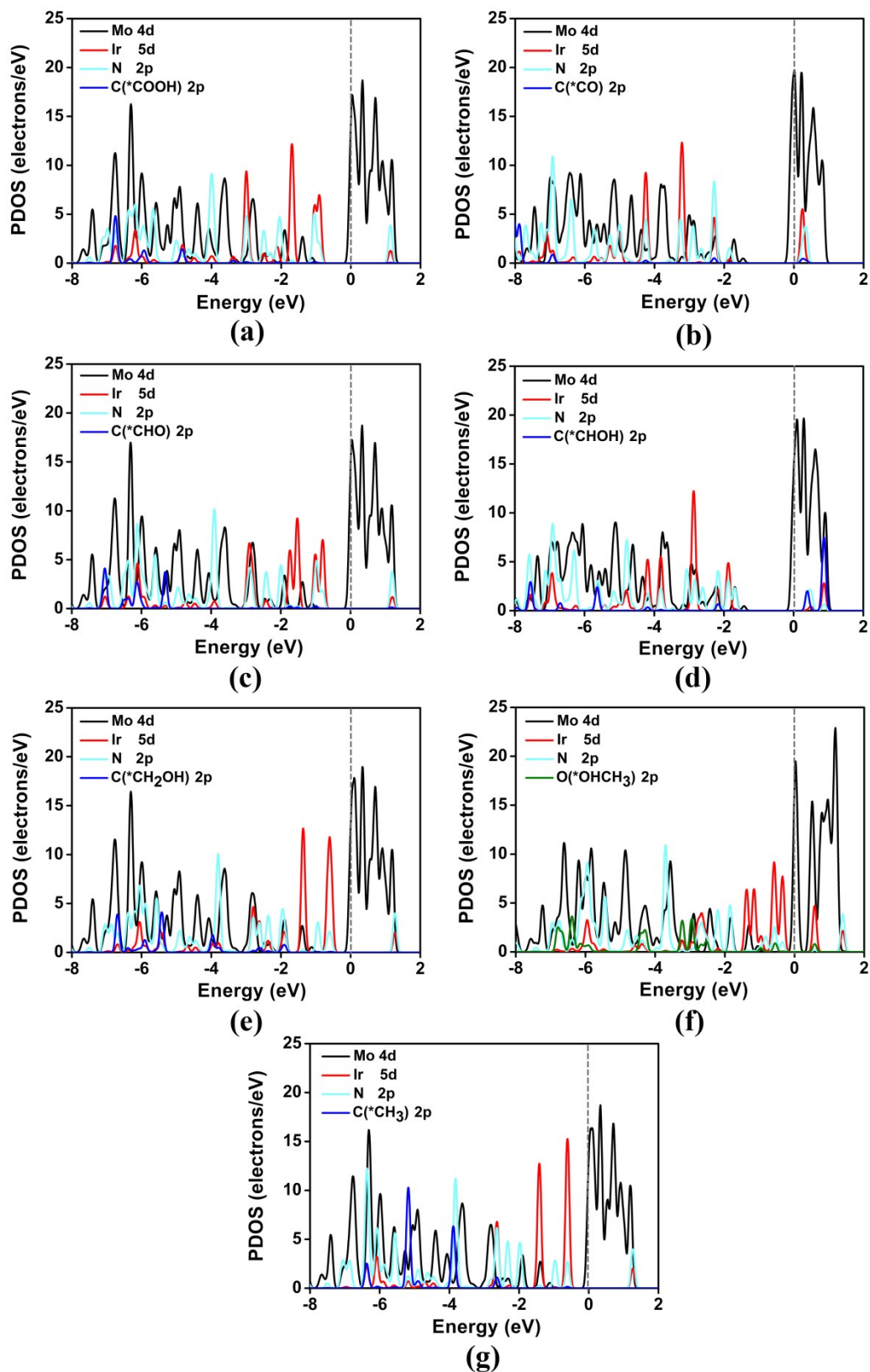
Fig. S14 The PDOS of 2D reductive Ir-PMOF adsorbing the intermediates of each step along the optimal reaction pathway: (a) *COOH, (b) *CO, (c) *CHO, (d) *CHOH, (e) *CH₂OH, (f) *OHCH₃, (g) *CH₃.
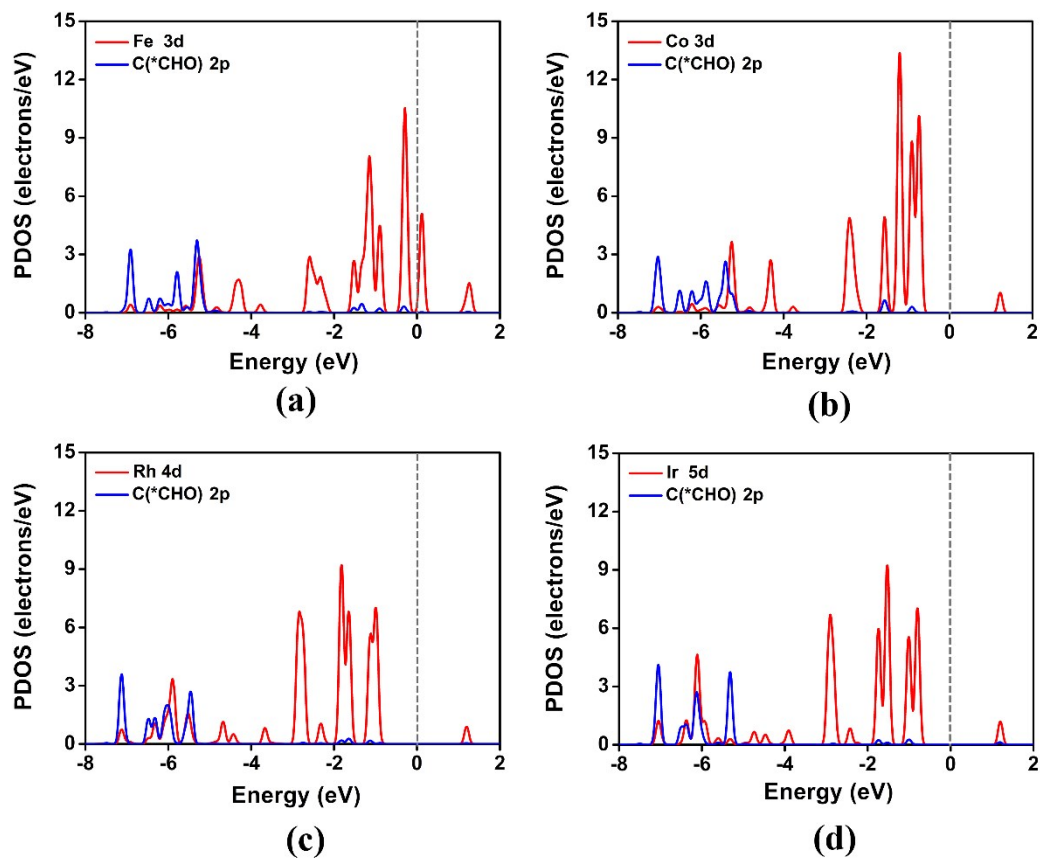
Fig. S15 The PDOS of *CHO intermediates adsorbed on 2D reductive (a) Fe-PMOF, (b) Co-PMOF, (c) Rh-PMOF, and (d) Ir-PMOF.
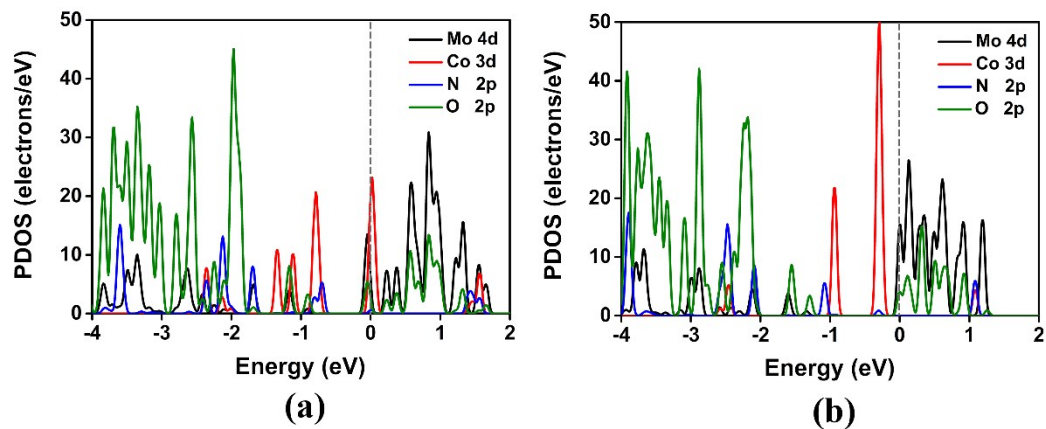
Fig. S16 The PDOS of reductive Co-PMOF (a) before and (b) after another electron acquisition.
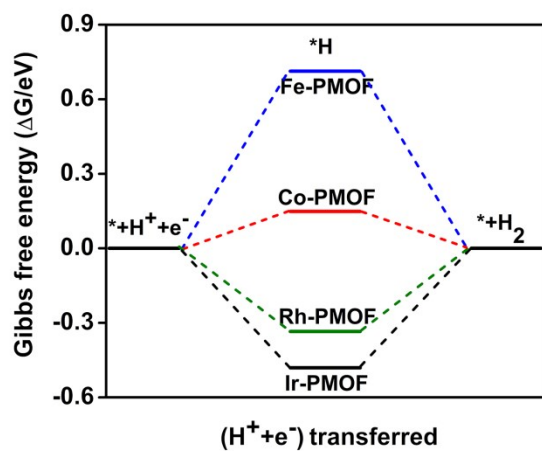
Fig. S17 The Gibbs free energy diagram of HER on 2D reductive TM-PMOF (TM = Fe, Co, Rh, Ir).

Table S2. The calculated adsorption energy (E_{ads}, eV), cohesive energy per atom (E_{coh}, eV) and formation energy (E_f, eV) of 2D reductive TM-PMOF (TM = Fe, Co, Rh, Ir).

	E_{ads}	E_{coh}	E_f
Fe-PMOF	-9.67	-5.62	-0.29
Co-PMOF	-9.40	-5.61	-0.29
Rh-PMOF	-9.72	-5.61	-0.29
Ir-PMOF	-5.70	-5.58	-0.24

For the TM-PMOF catalysts, the greater the adsorption energy (E_{ads}) of the transition metal (TM) atoms to the substrate (PMOF), the better the stability of the catalyst. The E_{ads} of these TM atoms (TM = Fe, Co, Rh, Ir) on the 2D PMOF substrate can be calculated according to $E_{ads} = E_{TM-PMOF} - E_{TM} - E_{PMOF}$, the computed E_{ads} values of Fe-PMOF, Co-PMOF, Rh-PMOF, Ir-PMOF are - 9.67, - 9.40, - 9.72, - 5.70 eV, respectively, indicating strong interactions between these TM atoms and the PMOF substrate. The E_{coh} is calculated from the equation $E_{coh} = (E_{tot} - aE_C - bE_N - cE_O - dE_H - eE_{Mo} - fE_{TM})/(a + b + c + d + e + f)$, where E_{tot}, E_C, E_N, E_O, E_H, E_{Mo}, and E_{TM} denote the energies of TM-PMOFs, isolated C, N, O, H, Mo, and TM atoms, respectively. The values of a-f are the numbers of C, N, O, H, Mo and TM atoms involved in the unit cell of TM-PMOFs, respectively. The E_f is also calculated according to $E_f = (E_{tot} - a\mu_C - b\mu_N - c\mu_O - d\mu_H - e\mu_{Mo} - f\mu_{TM})/(a + b + c + d + e + f)$, where μ_C, μ_N, μ_O, μ_H, μ_{Mo}, and μ_{TM} are the chemical potential of C, N, O, H, Mo, TM atoms, respectively. As shown in Table S2, the computed E_{coh} values of TM-PMOFs are lower than - 5 eV, confirming their high structural stability. Meanwhile, the calculated E_f values of TM-PMOFs are less than zero, which means that the studied TM-PMOFs are predicted to be relatively easy to synthesize experimentally.

Table S3. The optimal reaction pathways of 2D reductive TM-PMOF (TM = Fe, Co, Rh, Ir).

Reaction step	Reaction pathways
1	$* + CO_2 + H^+ + e^- \rightarrow *COOH$
2	$*COOH + H^+ + e^- \rightarrow *CO + H_2O$
3	$*CO + H^+ + e^- \rightarrow *CHO$
4	$*CHO + H^+ + e^- \rightarrow *CH_2O$ (or $*CHO + H^+ + e^- \rightarrow *CHOH$)
5	$*CH_2O + H^+ + e^- \rightarrow *CH_2OH$ (or $*CHOH + H^+ + e^- \rightarrow *CH_2OH$)
6	$*CH_2OH + H^+ + e^- \rightarrow *OHCH_3$
7	$*OHCH_3 + H^+ + e^- \rightarrow *CH_3 + H_2O$
8	$*CH_3 + H^+ + e^- \rightarrow * + CH_4$

Table S4. Charge states analyzed by Hirshfeld charge of the three moieties for 2D reductive Co-PMOF along the optimal reaction pathway. The moieties 1, 2, and 3 represent the adsorbed $C_xO_yH_z$, the $Co-N_4$ unit, and the Co-PMOF substrate, respectively. 0, 1, 2, 3, 4, 5, 6, and 7 represent the CO_2, $*COOH$, $*CO$, $*CHO$, $*CH_2O$, $*CH_2OH$, $*OHCH_3$, and $*CH_3$ intermediates along the reaction pathway.

Reaction step	Moiety 1	Moiety 2	Moiety 3
0	-0.0030	-0.2857	0.2887
1	-0.1499	-0.2516	0.4015
2	0.0376	-0.2525	0.2149
3	-0.0563	-0.2515	0.3078
4	-0.1351	-0.2495	0.3846
5	0.0199	-0.2200	0.2001
6	0.1821	-0.2262	0.0441
7	-0.0345	-0.2025	0.2370

The atomic coordinates of the optimized 2D reductive Co-PMOF system (provided in the format of Dmol³ input),

PBC parameters: a = b = 18.79 Å, c=30 Å, α = β = γ = 90°

atomic coordinates:

Co	9.3945	9.3945	15.0000
Mo	0.0000	0.0000	12.7776
Mo	0.0000	0.0000	17.2224
Mo	1.6889	17.1001	15.0000
Mo	17.1001	1.6889	15.0000
Mo	1.6953	1.6953	15.0000
Mo	17.0937	17.0937	15.0000
N	2.9376	15.8514	15.0000
N	15.8514	2.9376	15.0000
N	2.9448	2.9448	15.0000
N	15.8442	15.8442	15.0000
N	9.3966	7.4203	15.0000
N	9.3924	11.3687	15.0000
N	7.4203	9.3966	15.0000
N	11.3687	9.3924	15.0000
O	1.3313	17.4577	13.0812
O	17.4577	1.3313	13.0812
O	17.4577	1.3313	16.9188
O	1.3313	17.4577	16.9188
O	0.0142	16.0727	15.0000
O	18.7748	2.7163	15.0000
O	16.0727	0.0142	15.0000
O	2.7163	18.7748	15.0000
O	0.0000	0.0000	10.6712
O	0.0000	0.0000	19.3286
O	0.0000	0.0000	15.0000
O	1.3800	1.3800	16.9197
O	17.4090	17.4090	16.9197
O	1.3800	1.3800	13.0803
O	17.4090	17.4090	13.0803
C	14.8852	3.9038	15.0000
C	3.9038	14.8852	15.0000
C	14.3817	4.4073	16.2222
C	4.4073	14.3817	16.2222
C	4.4073	14.3817	13.7777
C	14.3817	4.4073	13.7777
C	8.2978	6.5690	15.0000
C	10.4912	12.2200	15.0000

C	6.5690	8.2978	15.0000
C	12.2200	10.4912	15.0000
C	8.7128	5.1914	15.0000
C	10.0762	13.5976	15.0000
C	5.1914	8.7128	15.0000
C	13.5976	10.0762	15.0000
C	10.0771	5.1903	15.0000
C	8.7119	13.5987	15.0000
C	5.1903	10.0771	15.0000
C	13.5987	8.7119	15.0000
C	10.4946	6.5669	15.0000
C	8.2944	12.2221	15.0000
C	6.5669	10.4946	15.0000
C	12.2221	8.2944	15.0000
C	11.8328	6.9562	15.0000
C	6.9562	11.8328	15.0000
C	12.8906	5.8984	15.0000
C	5.8984	12.8906	15.0000
C	13.3956	5.3934	13.7889
C	5.3934	13.3956	13.7889
C	5.3934	13.3956	16.2110
C	13.3956	5.3934	16.2110
C	3.9101	3.9101	15.0000
C	14.8789	14.8789	15.0000
C	4.4139	4.4139	16.2222
C	14.3751	14.3751	16.2222
C	4.4139	4.4139	13.7777
C	14.3751	14.3751	13.7777
C	11.8286	11.8286	15.0000
C	6.9604	6.9604	15.0000
C	5.9039	5.9039	15.0000
C	12.8851	12.8851	15.0000
C	5.3996	5.3996	16.2120
C	13.3894	13.3894	16.2120
C	5.3996	5.3996	13.7880
C	13.3894	13.3894	13.7880
H	0.5636	0.5636	10.1066
H	18.2254	18.2254	10.1066
H	0.5636	0.5636	19.8933
H	18.2254	18.2254	19.8933
H	13.0108	5.7782	17.1573
H	5.7782	13.0108	17.1573
H	5.7782	13.0108	12.8427
H	13.0108	5.7782	12.8427

H	14.7714	4.0176	17.1630
H	4.0176	14.7714	17.1630
H	4.0176	14.7714	12.8369
H	14.7714	4.0176	12.8369
H	8.0325	4.3444	15.0000
H	10.7565	14.4446	15.0000
H	4.3444	8.0325	15.0000
H	14.4446	10.7565	15.0000
H	10.7560	4.3421	15.0000
H	8.0330	14.4469	15.0000
H	4.3421	10.7560	15.0000
H	14.4469	8.0330	15.0000
H	5.7855	5.7855	17.1573
H	13.0035	13.0035	17.1573
H	5.7855	5.7855	12.8427
H	13.0035	13.0035	12.8427
H	4.0234	4.0234	17.1624
H	14.7656	14.7656	17.1624
H	4.0234	4.0234	12.8376
H	14.7656	14.7656	12.8376

Supplementary References

1 B. Delley, *J. Chem. Phys.,* 1990, **92**, 508-517.

2 B. Delley, *J. Chem. Phys.,* 2000, **113,** 7756-7764.

3 J. P. Perdew, K. Burke and M. Ernzerhof, *Phys. Rev. Lett.,* 1996, **77,** 3865-3868.

4 B. Delley, *Phys. Rev. B: Condens. Matter Mater, Phys.,* 2002, **66**, 155125-155133.

5 S. Grimme, *J. Comput. Chem.,* 2006, **27**, 1787-1799.

6 F. L. Hirshfeld, *Theor. Chim. Acta,* 1977, **44**, 129-138.

7 J. K. Nørskov, J. Rossmeisl, A. Logadottir, L. Lindqvist, J. R. Kitchin, T. Bligaard and H. Jónsson, *J. Phys. Chem. B,* 2004, **46**, 17886-17892.

8 J. Rossmeisl, A. Logadottir and J. K. Nørskov, *Chem, Phys.,* 2005, **319**, 178-184.

9 J. Zhao, J. X. Zhao, F. Y. Li and Z. F. Chen, *J. Phys. Chem. C,* 2018, **122**, 19712-19721.

10 J. H. Liu, L. M. Yang and E. Ganz, *J. Mater. Chem. A,* 2019, **7**, 3805-3814.

11 J. H. Liu, L. M. Yang and E. Ganz, *ACS Sustainable Chem. Eng.,* 2018, **6**, 15494-15502.

12 Computational Chemistry Comparison and Benchmark Database. http://cccbdb.nist.gov/.

13 Y. R. Wang, Q. Huang, C. T. He, Y. F. Chen, J. Liu, F. C. Shen and Y. Q. Lan, *Nat. Commun.,* 2018, **9**, 4466.

14 Q. Huang, J. Liu, L. Feng, Q. Wang, W. Guan, L. Z. Dong, L. Zhang, L. K. Yan, Y. Q. Lan and H. C. Zhou, *Nati. Sci. Rev.,* 2020, **7**, 53-63.

15 F. Y. Yu, Z. L. Lang, L. Y. Yin, K. Feng, Y. J. Xia, H. Q. Tan, H. T. Zhu, J. Zhong, Z. H. Kang and Y. G. Li, *Nat. Commun.,* 2020, **11**, 490.

16 J. Du, Z. L. Lang, Y. Y. Ma, H. Q. Tan, B. L. Liu, Y. H. Wang, Z. H. Kang and Y. G. Li, *Chem. Sci.,* 2020, **11**, 3007-3015.